CHAPTER ONE

GENERAL INTRODUCTION

1.1 INTRODUCTION

Columbus Stainless is the primary manufacturer of flat cast and wrought stainless steel products in Southern Africa. One of the growth sectors in the use of stainless steels is in the automotive components industry and more particularly, in catalytic converters in the automotive industry. The manufacture of automobile emission control systems in South Africa is one of the fastest growing industry sectors in the world. Founded on the growth and development of catalytic converters, South Africa supplies in excess of 10% of the world's production, mainly stemming from its dominance in PGM (Platinum Group Metals) production. Catalytic converters are the largest of the auto component groupings being exported from South Africa and now amount to $500 million/year. The growth of the local catalytic converter industry has been spectacular, see Figure 1.1.

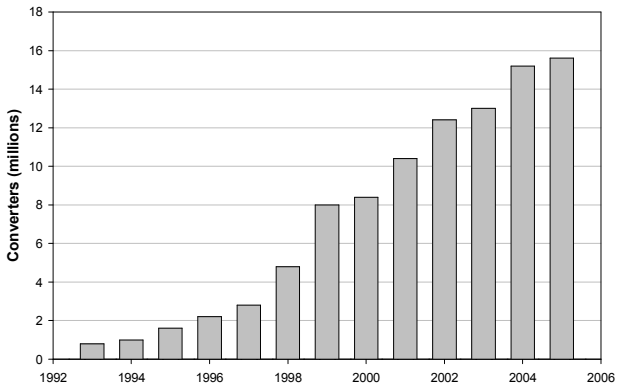

Figure 1.1. Catalytic converters growth industry in South Africa [1].

The operating temperatures for catalytic converters are in the region of 900°C but are associated with a frequent temperature variation as automobiles are used intermittently. Thus, the material for this application requires excellent thermal fatigue resistance and high temperature strength. The primary steel used in this application is type 441 stainless steel, (which is equivalent to DIN 1.4509). This steel is fully ferritic over a wide range of temperatures. Type 441 is a dual stabilised (titanium and niobium) ferritic stainless steel with 18 wt% chromium, and the typical composition of this steel is shown in the Table 1.1 below. Titanium and Niobium carbides are more stable than chromium carbides and prevent the formation of chromium carbides on grain boundaries (which

results in sensitisation of the alloy in near grain boundary regions). The dual stabilisation by both Ti and Nb imparts beneficial corrosion resistance, oxidation resistance, high temperature strength and formability to the steel [2].

Table 1.1. A typical chemical composition (wt%) of type 441 ferritic stainless steels.

	C	N	Mn	Si	Cr	Ni	Ti	Nb	S	P	Remarks
Min					17.50		0.10				%Nb≥ 3xC + 0.3
Max	0.03	0.045	1.00	1.00	18.50	0.50	0.60	1.00	0.015	0.04	

Many researchers have investigated the effects of niobium stabilisation on ferritic stainless steels for their use in automotive exhaust systems [3,4,5,6], and have found that niobium additions can improve the high temperature strength of ferritic stainless steels by solid solution strengthening, which allows its operation at such high temperatures. It is, therefore, important to know how much of the niobium precipitates out as carbides or carbo-nitrides and which fraction remains in solution. Niobium stabilised ferritic stainless steels form the precipitates of Nb(C,N), M_6C (Fe_3Nb_3C) and the Laves phase type Fe_2M (Fe_2Nb).

Because C and N remain in the steels, Nb(C,N) and Ti(C,N) are easily formed in some processing stages, e.g. in hot–rolling and annealing processes. These carbo – nitrides increase the strength and decrease both the toughness and ductility. In the work by Fujita et al. [5], on 13Cr – 0.5Nb, the authors have observed that the high temperature strength of Nb added steels decreases during high temperature ageing, caused by coarse M_6C (Fe_3Nb_3C) formation in ageing.

The volume fraction of the Laves phase was observed to reach a maximum at 700°C and its dissolution occurs at temperatures over 900°C [7,8]. The same observation has been made by the use of thermodynamic software such as Thermo-calc® [3, 9]. The Laves phase precipitates firstly at the grain boundaries as a fine precipitate and as the steel is slowly cooled from a high temperature of about 900°C, the amount of this Laves phase increases inside the grains and they then coarsen. This intermetallic Laves phase is known to affect both the mechanical properties and corrosion resistance of ferritic stainless steel, mostly negatively. In one instance, it has been found that the fine precipitates of Laves phase at the grain boundaries improve the high temperature strength when still fine [5]. However, the rapid coarsening of the Laves phase at high temperatures reduced the high temperature strength [10]. The exact mechanism of strength reduction is still not clear and requires clarification. Sawatani et al [8], researched the effect of Laves phase on the properties of dual stabilised low carbon

stainless steels as related to the manufacturing process of Ti- and Nb-stabilised low C, N-19%Cr-2%Mo stainless steel sheets, and they have found that the Laves phase has a significant influence on the mechanical properties of the steel. It was found that Laves phase on the grain boundaries shifts the brittle to ductile transition temperature to higher temperatures, and that large amounts of Laves phase degrade the room temperature ductility of cold rolled and annealed sheet and greatly enhance its strength. It was also observed that after a 20% cold rolled reduction (of a sheet that had been cold rolled and annealed after reductions between 0 and 92%) that there was a peculiarly rapid precipitation of Laves phase, which caused a severe degradation of the mechanical properties [11].

1.2 Problem Statement

Columbus Stainless has experienced an embrittlement problem at times during the manufacturing process of type 441 stainless steel. This problem is considered generic because it appears from the hot band material prior to annealing, whereby the materials become embrittled after hot rolling and coiling. It was assumed that the embrittlement might be attributed to the formation of an intermetallic Laves phase type. The reason for this assumption is that after the hot finishing mill (Steckel mill), the temperature of the steel strip is approximately 850°C, and the strip is then rapidly cooled (to avoid the Laves phase transformation temperature range) to approximately 650°C by means of laminar cooling with water sprays on the run-out table and is then coiled. The coil is left to cool for 3 to 5 days to approximately 50°C before further processing. For instance, one particular hot rolled coil was found to be brittle and could not be processed further. It appears furthermore that rapid cooling (by water sprays) after hot rolling alleviates the embrittlement problem, and that slow cooling of this particular hot rolled coil might have allowed the precipitation of the Laves phase below 650ºC and that this resulted in the embrittlement of the material. Also, the preliminary evaluation by Columbus Stainless of this steel indicated that this embrittlement is not related to a coarse ferritic grain size effect, as the degree of embrittlement was far higher than expected from this source.

1.3 Objectives

Laves phase precipitation is believed to be detrimental to mechanical properties, in particular leading to a low toughness in this type of steel. The following two objectives have been identified:

1. Firstly, by making use of this reject material, to determine those process variables that may affect the toughness of the material after processing, principally annealing temperatures and cooling rates from typical hot rolling temperatures; and

2. To model and experimentally determine the kinetics of precipitation of this phase, since it would then be possible to predict what volume fraction of Laves phase forms firstly, during processing and secondly, what forms possibly throughout the component's lifetime in exhaust systems.

The type 441 steel (composition shown in Table 1.1) is susceptible to Laves phase formation over a relatively wide temperature range. A number of studies of Laves phase precipitation in this steel provide suitable experimental data with which to test the precipitation model [12].

CHAPTER TWO

LITERATURE REVIEW

2.1 INTRODUCTION

Stainless steels are iron-base alloys containing a minimum of 11wt.% chromium content for adequate corrosion resistance. This chromium content is the minimum that prevents the formation of "rust" in air or in polluted atmospheres by forming a very thin surface film of chromium oxides known as the "passive film", which is self-healing in a wide variety of environments. Today, the chromium content in stainless steels approaches 30wt.% in some alloys and other elements are often added to provide specific properties or ease of fabrication. Some of these elements are nickel (Ni), nitrogen (N) and molybdenum (Mo) which are added for corrosion resistance; carbon (C), Mo, N, titanium (Ti), aluminium (Al) and copper (Cu) which are added for strength; sulphur (S) and selenium (Se) are added for machinability; and Ni is added for formability and toughness, particularly to obtain an austenitic microstructure which is far less prone to the loss of toughness from a large grain size.

2.2 CLASSIFICATION OF STAINLESS STEELS

Stainless steels are divided into three groups according to their crystal structures: austenitic (face-centred cubic, fcc), ferritic (body-centred cubic, bcc) and martensitic (body-centred tetragonal or cubic, bct). Stainless steels containing both austenite and ferrite usually in roughly equal amounts are known as "duplex stainless steels".

The general considerations for the choice of the base metal are that it should have the following properties: (a) since these alloys are used at high temperatures or under demanding conditions, they should have adequate corrosion resistance. This implies that either Cr or Al at a level of about 15% or higher, should be added to the alloy. (b) The room temperature structure should be austenitic, primarily to avoid the formation of martensite during cooling to room temperature and secondly, to prevent a ferritic structure which has a lower solubility for carbon and favours the formation of intermetallic precipitates rather than carbides. The addition of austenite formers (mainly Ni, Mn and N) is, therefore, necessary in austenitic stainless steels.

The Fe-Cr-Ni system as the base alloy is by far the most suitable as large quantities of Cr can be taken into solution and maintained in solution down to room temperature. Secondly, Ni is also a strong austenite former and Cr lowers the martensite start (M_s) temperature sufficiently to avoid the formation of martensite, see Figure 2.1.

Both nitrogen and carbon are strong austenite formers, with nitrogen being increasingly used to provide certain attractive properties such as good fracture strength and it also improves the corrosion resistance [13,14]. From Figure 2.2, it is noted that carbon is a very strong austenite former, and if the carbon content is very low, slightly more Ni may have to be added to compensate for the loss of the austenitic properties of the carbon.

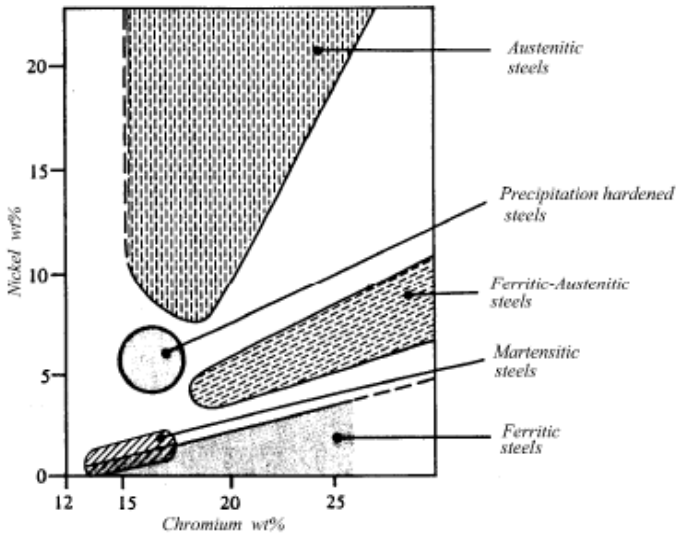

Figure 2.1. The effect of nickel and chromium content on the structure of the main stainless steels. Note in particular that Ni is a strong austenite former whereas Cr is a strong ferrite former [15].

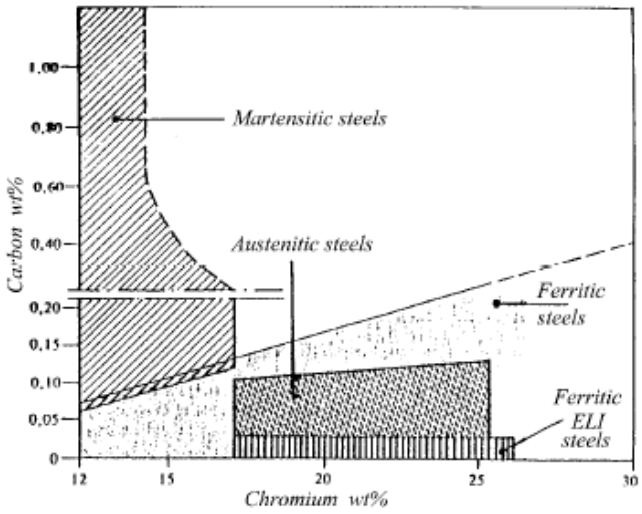

Figure 2.2. Effect of carbon and chromium contents on the structure of some of the main stainless steels. ELI is extra low interstitial steel [15].

2.2.1 Ferritic Stainless Steel

This stainless steel derives its name from the bcc crystallographic structure that is generally stable from room temperature up to the liquidus temperature. Typically, ferritic stainless steel contains approximately 11 to 30wt.% chromium and small amounts of other alloying elements. The chromium additions give the steel its corrosion resistance and it further stabilises the bcc crystal structure. Recently, a very low (C+N) content has been specified in the so-called super-ferritic stainless steels. The higher alloy compositions can also include up to 4%Ni, provided this does not alter their fully ferritic structure. Due to their adequate corrosion resistance and lower cost, ferritic stainless steels are chosen over austenitic stainless steels in less severe applications such as a replacement to mild carbon steels in automobile exhaust systems. However, poor weldability, which leads to low toughness and is also associated with grain growth in the HAZ, limits their use even with very low carbon levels.

2.2.2 Austenitic Stainless Steel

As with ferritic steel, the austenitic stainless steel's name originates from its fcc crystallographic structure. These steels contain 16 to 25wt% chromium and 7 to 10% nickel. Austenitic stainless steel has a high nickel content to stabilise the austenite fcc structure at room temperature. The increase in alloy content creates a higher cost of production but the fcc structure exhibits very high ductility, resulting in material with good formability and very good corrosion resistance. Another advantage of these steels is the relative ease of recrystallisation, which allows for better control of the mechanical properties.

2.2.3 Martensitic Stainless Steel

Martensitic stainless steels contain 12 to 17% chromium for good corrosion resistance. However, since chromium is a strong ferritic stabiliser, austenite stabilisers are added so that the necessary austenite can be formed during solution treatment for the subsequent martensite formation. Therefore, these steels have a high carbon content to stabilise the austenite at higher temperatures. The high carbon content will increase the strength through solid solution strengthening and the precipitation of a large number of (Fe, Cr) carbides. These steels use the quench and temper process to achieve a very high strength with reasonable ductility. Because of the high alloy content, these steel have a superior hardenability. The disadvantage of the high hardenability often leads to

degradation of the corrosion resistance when compared with ferritic and austenitic stainless steels.

2.2.4 Duplex Stainless Steel

These steels contain a mixture of ferrite and austenite phases at room temperature in order to combine the beneficial properties of both components. These steels typically contain 18 to 30% chromium and an intermediate amount of nickel (3-9%) that is not enough for the formation of a fully austenitic structure at room temperature. Duplex stainless steels have an intermediate level of high mechanical strength and corrosion resistance properties lying between those of austenitic and ferritic products.

2.3 Composition of Stainless Steels

The composition of stainless steel can be related to its non-equilibrium metallurgical structure by means of a Schaeffler diagram [16], which shows the microstructure obtained after a rapid cooling from 1050°C to room temperature. It is, therefore, not an equilibrium diagram and is often used in welding phase analysis. This diagram was originally established to estimate the amount of delta ferrite (that is, ferrite formed on solidification, as opposed to alpha ferrite, which is a transformation product of austenite or martensite) content of welds in austenitic stainless steels. The alloying elements commonly found in stainless steels are regarded either as austenite stabilisers or as delta ferrite stabilisers. The relative “potency” of each element is conveniently expressed in terms of an empirical equivalence to either nickel (austenite stabiliser) or chromium (ferrite stabiliser) on a weight percentage basis. The nickel and chromium equivalents, which form the two axes of the Schaeffler diagram, can be calculated as follows:

$$\%Ni\ equivalent = \%Ni + \%Co + 30\%C + 25\%N + 0.5\%Mn + 0.3\%Cu$$

$$\%Cr\ equivalent = \%Cr + 2\%Si + 1.5\%Mo + 5\%V + 5.5\%Al + 1.75\%Nb + 1.5\%Ti + 0.75\%W$$

2.3.1 Structure of Ferritic Stainless Steel

Ferritic stainless steels at room temperature consist of alpha (α) solid solution having a body centred cubic (bcc) crystal structure. The alloy contains very little interstitial carbon and nitrogen in solution; most of the interstitial elements appear as finely distributed carbides and nitrides. A typical phase diagram of the iron-chromium system is shown in Figure 2.3.

Chromium is a ferrite stabiliser and it extends the alpha-phase field and suppresses the gamma-phase field. This results in the formation of the so-called gamma loop as seen in Figure 2.3, which, in the absence of carbon and nitrogen, extends to chromium contents of about 12 – 13wt % [17]. At the higher chromium contents, transformation to austenite is no longer possible and the metal will remain ferritic up to its melting temperature. This constitutes an entirely different class of stainless steels in which grain refinement can no longer be brought about by transformation through heat treatment.

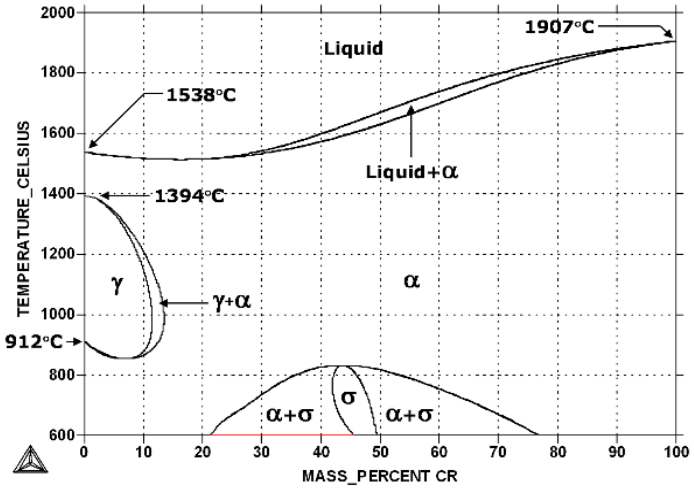

Figure 2.3. Fe-Cr equilibrium phase diagram [17].

With carbon and nitrogen present in these alloys the diagram is modified in certain respects. The effect of carbon and nitrogen is to shift the limits of the gamma loop to higher chromium contents and widens the duplex (α + γ) phase area [18]. Figure 2.4 shows the changes in this part of the diagram. However, the solubility levels of the interstitials in the ferrite matrix are sufficiently low so that it is rarely possible to distinguish between solute embrittling effects and the effects of second-phase precipitates. The precipitates, in fact, become more important than the solute when the amount of interstitial elements significantly exceeds the solubility limit. The presences of carbon or nitrogen, in amounts in excess of the solubility limit, serve to increase the ductile to brittle transition temperature (DBTT). This embrittling effect is closely linked to the amount or the number and size of carbides and nitrides formed on the grain boundaries but also to the ferrite grain size. Precipitate films act as strong barriers to slip propagation across the grain boundaries and are also often inherently brittle by themselves. Grain boundary precipitates are suppressed by quenching from above the solution temperature when the interstitial content is low enough.

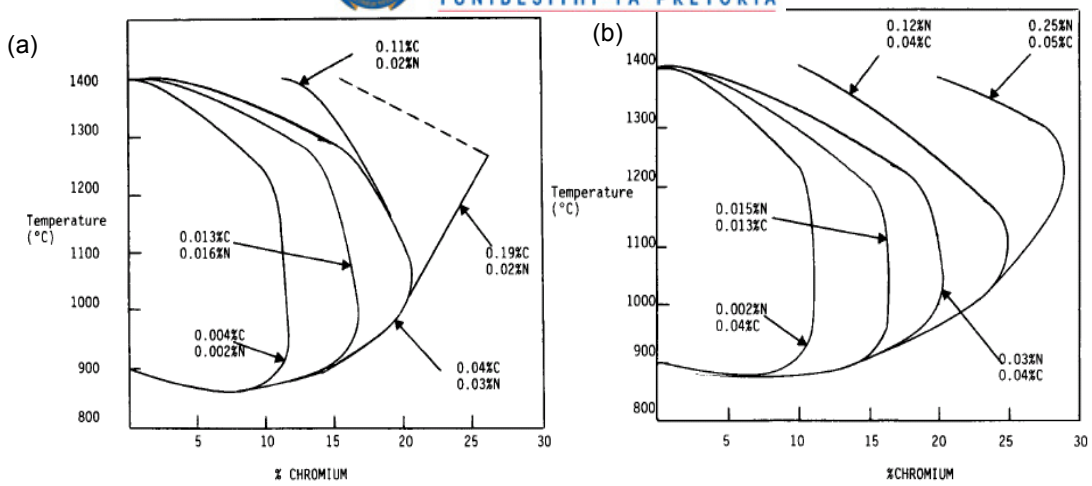

Figure 2.4. Shifting of the boundary line ($\alpha + \gamma$)/γ in the Fe-Cr system through additions of C + N [18].

2.4 TOUGHNESS OF FERRITIC STAINLESS STEELS

Some of the metallurgical problems that are encountered in the ferritic stainless steels are too large a grain size, “475°C” embrittlement, secondary phase precipitation, high-temperature embrittlement and notch sensitivity. They all have been shown to some extent to affect the ductile–to–brittle transition temperature of the ferritic stainless steels, mostly negatively by raising it.

2.4.1 EFFECT OF GRAIN SIZE ON BRITTLE BEHAVIOUR

The effect of grain size on the impact toughness of ferritic stainless steels has been well documented over the years even though it is not always clearly understood. It has been proven previously that the DBTT tends to increase with increasing grain size, see Figure 2.5 [18,19]. The work done by Ohashi et al [20] has shown that while the transition temperature increases with increasing grain size, the upper shelf energy is largely independent of the grain size. They have also reported that in V–notched samples that the effect of grain size is very noticeable; but in brittle welded samples this grain size dependency of the upper shelf energy and the DBTT is very small but still observable. It can be concluded that the coarse grain size tends to promote crack initiation even in a blunt–notched specimen, but the grain size effect contributes mainly to the resistance of initiation of brittle fracture and only slightly to the propagation of brittle fracture [20].

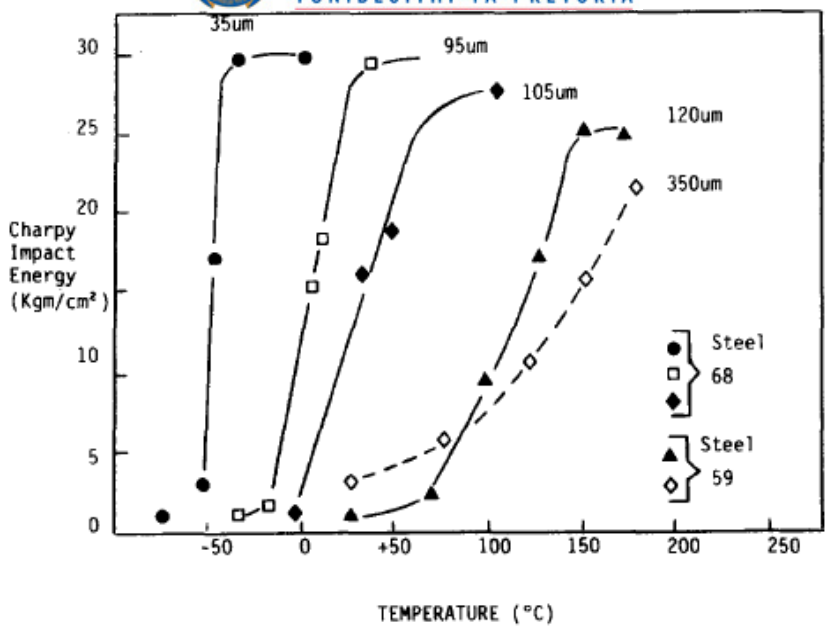

Figure 2.5. The effect of the grain size on the impact toughness for several Fe – 25Cr ferritic stainless steels. Steel 59 and 68 are the alloy numbers [18].

Figure 2.6 shows the impact transition temperature as a function of the interstitial content for two different ferritic stainless steels [21]. For a given interstitial content, both the DBTT and the upper shelf energies were not affected by the presence of 2% Mo or the change of Cr content from 18% to 25%. These findings agree with the results of Woods [22], who showed that for 18% Cr in Ti stabilised stainless steels, that 2% Mo has no effect on the impact transition temperature.

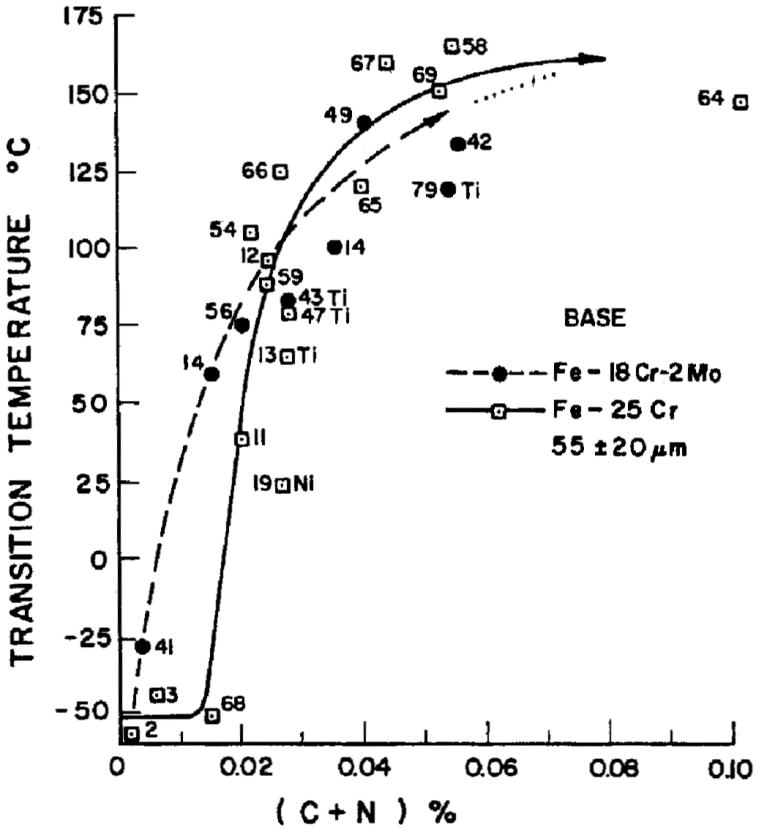

Figure 2.6. The effect of the interstitial content on the impact transition temperature for the Fe–18Cr–2Mo and Fe–25Cr steels with the grain sizes within the range 35 to 75 μm. The numbers given correspond to the alloy number [21].

For a desirable low DBTT and a high shelf energy, the combined carbon and nitrogen content should be kept below 150 ppm, below which further decreases have no further effect. Above150 ppm, however, increases in interstitial content cause a marked increase in DBTT, though once above a certain level (C + N ≈ 600 ppm) further increases are not significant. For these stainless steels a room temperature Charpy Impact Energy (CIE) value of between 14 to 70 J, and above the DBTT a value of 160J in the Upper Shelf Energy region, would be considered typical [21].

2.4.2 EMBRITTLEMENT AT 475°C

When ferritic stainless steels containing at least 12wt.% chromium are subjected to prolonged exposure to temperatures between 400 and 500°C, the notch ductility is considerably reduced while the tensile strength and hardness increase considerably. However, the increase in the tensile strength is of no practical significance since the alloy is extremely brittle [18,19]. This phenomenon is known as “475°C” embrittlement because the maximum effect occurs at about 475°C [23]. Brittle fracture is transgranular in nature and is similar in appearance to the low temperature cleavage of unembrittled

steels [24]. Transgranular fracture is observed to initiate at the interaction of slip bands with grain boundaries. However, the precise mechanism of the crack nucleation by slip bands has not been resolved experimentally [24]. The recognised mechanism of "475°C" embrittlement is the precipitation through spinodal "unmixing" of Cr-rich alpha prime (α') and Fe-rich α phases, arising from the miscibility gap in the Fe-Cr equilibrium phase diagram, Figure 2.3. The kinetics of α' precipitation increase with increasing Cr content. A spinodal phase mixture exists within the miscibility gap, and the precipitation of the α' is thought to occur by a nucleation and growth mode outside the spinodal boundaries and by spinodal decomposition within [19,23].

The phenomenon of "475°C" embrittlement can be removed by heating the embrittled alloy to a temperature above 550°C for a sufficient amount of time to dissolve the α' phase followed by rapid cooling to room temperature.

2.4.3 Precipitation of the Secondary Phases in Stainless Steels

Ferritic stainless steel in the temperature range of 500 to 900 °C can also precipitate intermetallic phases such as sigma (σ), chi (χ) and Laves phases. From the Fe-Cr equilibrium phase diagram in Figure 2.3, it can be seen that sigma phase (σ) is an equilibrium phase at temperatures up to 820 °C. The sigma (σ) phase is an intermetallic compound with approximate composition of FeCr. It is hard and brittle and can result in a severe harmful influence on the toughness properties of the alloys. Although the stability range of this phase in the Fe-Cr binary system varies from 519 to 820°C, several substitutionally dissolved elements can markedly modify this temperature range. Substitutional elements such as Mo, Si and Ni shift the σ-phase boundary to a lower chromium range [18,19]. On the other hand, the precipitation of sigma phase can be strongly accelerated by the pre-existence of carbides in the alloy, particularly the $M_{23}C_6$ type [25,26,27,28]. In the lower Cr content ferritic stainless steels, sigma phase forms very slowly and is usually a service problem only after a long exposure at elevated temperatures. Cold work enhances the precipitation rate of the sigma phase considerably, and in very high chromium containing steels sigma phase has been found in an air cooled as-cast structure [18,23]. Increasing the chromium and molybdenum contents favours the formation of sigma, chi and Laves phases.

The relationship between the toughness and the Fe_2Mo Laves phase precipitates in a 9%Cr – 2%Mo ferritic martensitic steel was investigated by Hosoi et al. [29]. They

observed that the DBTT increases and the upper shelf energy decreases when the Laves phase begins to precipitate during ageing.

2.4.4 NOTCH SENSITIVITY

Sensitisation in ferritic stainless steels occurs whenever the steel is heated to a sensitising temperature (usually above 900°C), such as during thermo-mechanical processing and/or welding. The precipitation of $M_{23}C_6$, an incoherent carbide with a complex cubic structure, usually occurs on the grain boundaries, which then form Cr-depleted zones along the grain boundary and places the alloy in the sensitised state, resulting in intergranular corrosion adjacent to the grain boundaries when exposed to corrosive environments. A sketch showing the carbides and the associated chromium-depleted zones along the grain boundaries is shown in Figure 2.7. Precipitation of chromium nitrides such as Cr_2N requires slow cooling through a temperature range of 500 to 700°C. Above 700°C, the diffusion of chromium is fast enough to replenish the chromium at the grain boundaries and below 500°C, the diffusion of chromium is too slow for the precipitates to form in nitrogen containing alloys. One place where this slow cooling can occur is in the heat-affected zone (HAZ) in the vicinity of a weld joint.

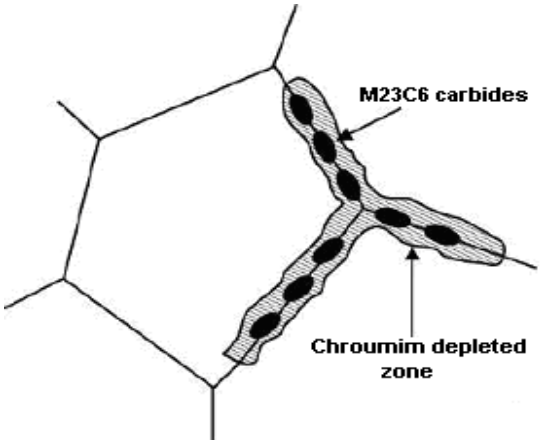

Figure 2.7. A schematic diagram of the grain boundary showing carbides in the chromium-depleted zone near the grain boundaries.

Sensitisation can be overcome by one of several methods, all of which increase production cost:

- Annealing alloys at temperatures between 950 and 1100°C in the austenite regions, allowing Cr to rediffuse back into the Cr-depleted zones.

- Retard the kinetics of sensitisation through molybdenum (Mo) additions, which lengthens the time required for sensitisation by slower diffusion of the Mo which is then thermodynamically built into the M part of $M_{23}C_6$.

- Reduce interstitial levels by better control during steelmaking processes.

- "Free" carbon and nitrogen levels can be further reduced by the addition of strong carbide and nitride forming elements such as the stabilisers Ti, Nb and Zr, thereby reducing the formation of the Cr-rich $M_{23}C_6$.

2.4.5 Weldability of Ferritic Stainless Steel

The problem faced in joining ferritic stainless steels is grain growth to coarse grain sizes in the weld zone and the heat-affected zone of fusion welds, and consequently low toughness and ductility due to the absence of any phase transformations during which grain refinement can occur. In general, austenitic stainless steels are easily weldable. When austenitic stainless steel joints are employed in cryogenic and corrosive environments, the quantity of delta-ferrite in the weld must be minimised or controlled to avoid degradation during service [30].

It has been shown that the addition of niobium and titanium to stabilise the steel does not adversely affect the weldability of the steel. The addition may in fact increase the toughness in titanium stabilised steel [31,32]. In addition dual stabilisation was found to produce tough, clean weld lines during high frequency welding when compared to only single titanium stabilised steels. An optimum balance or ratio normally exists between the titanium and niobium content (with the niobium being the greater i.e. Nb:Ti shown to be 2:1 for a 17% chromium ferritic steel) for optimum toughness and ductility of welds [33]. Finally it has been shown that dual stabilised steels can be susceptible to intergranular hot cracking in the fusion and heat-affected zones. It has been shown that niobium is in fact the most deleterious element and care should be taken to minimise this stabilising element as far as possible [23].

2.4.6 Effect of Niobium and Titanium Additions to Ferritic Stainless Steels

Redmond [34] has investigated the effects of residual and stabilising elements on the toughness of a series of 18%Cr-2%Mo steels which contained 0.015%C and 0.015%N. The residual elements that were varied were sulphur, manganese and silicon and they all were shown to have only a minor effect on the impact toughness. The effects of

niobium and titanium dual stabilisation on the impact toughness are shown in Figure 2.8. From this figure it can be seen that as for base metal materials, increasing the titanium content resulted in a constant increase in the transition temperature. For the alloys with 0.34 and 0.44%Nb the maximum for both occurs at about 30°C for 0.2%Ti. The trend is less clear when the niobium content was varied and the titanium content was kept constant. In the welded condition, the trend still does not correlate well with the niobium content. The niobium stabilised steel had a better impact toughness than the titanium stabilised steel, with a mixed niobium-titanium stabilisation producing results between the two [34].

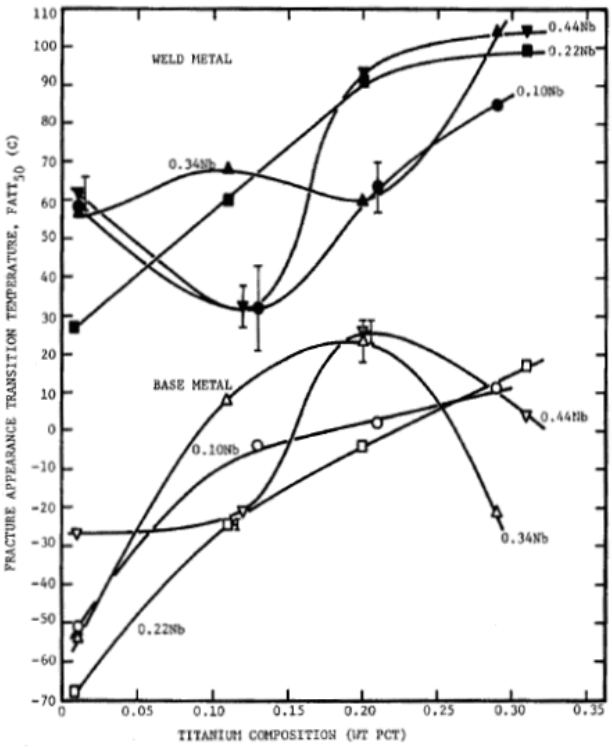

Figure 2.8. Effect of niobium and titanium additions on the impact toughness of 18%Cr-2%Mo ferritic stainless steels [34].

2.5 THEORIES OF BRITTLE FRACTURE

Brittle fracture of steel structures has been a matter of considerable concern to both engineers and metallurgists for many years, it now being generally recognised that the cleavage mode of failure occupies a central position with respect to the problem. A physical model of the process has thereby been constructed by others [35], and in so doing, previous theories were critically examined. The first of these contributions was the identification of the crack initiators from which cleavage nucleates and triggers a propagating crack in a ferritic matrix, together with the criterion for this to occur. Stroh

[36,37] proposed a wedge dislocation pile-up at a grain boundary as the initiator, Cottrell [38] a sessile wedge dislocation pile-up resulting from dislocation coalescence, and Smith [39] the combination of a wedge dislocation pile-up at a grain boundary with a contiguous brittle second-phase particle or inclusion, broken by the pile-up. All these initiators are able to nucleate a crack at a neighbouring ferrite grain if assisted by plastic flow, while the last two are also able to propagate the nucleus of the crack once formed if assisted by the stress state. An energy balance involving the effective surface energy of the metallic matrix and the initiator size (the ferritic grain, the second-phase particle, etc.) allows the tensile stress required for propagating the nucleus to be derived, thus predicting the maximum principal stress that triggers cleavage and provides a cleavage fracture criterion.

2.5.1 ZENER'S/STROH'S THEORY

Zener [ref. by Chell, 40] suggested that the local stress concentration produced at the head of a dislocation pile – up could lead to cleavage fracture when the leading dislocations were squeezed together to generate a stress concentration leading to a crack nucleus. The model shows that the crack nucleation of length $2c$ (see Figure 2.9) occurs when the shear stress τ_s created by a pile – up of n dislocations of Burger's vector b each at the grain boundary, reaches the value of:

$$\tau_s \approx \tau_i + \left(\frac{2\gamma_s}{nb}\right) \qquad \text{Equation 2.1}$$

where τ_i is the lattice friction stress in the slip plane and γ_s is the surface energy of the exposed crack surface.

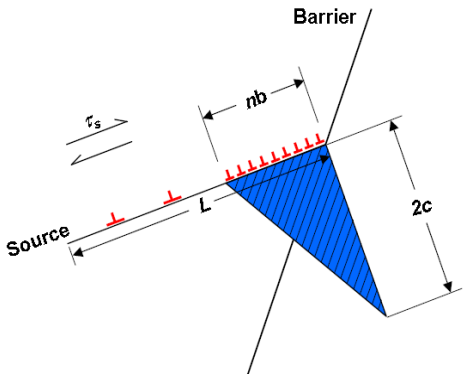

Figure 2.9. Zener's model for cleavage fracture.

Stroh [36] included the effect of the grain size d in a model, suggesting the condition for the shear stress created by a dislocation pile – up of length $d/2$ to nucleate a microcrack as follows (Figure 2.10):

$$\tau_e = \tau_y - \tau_i \geq \sqrt{\frac{E\pi\gamma}{4(1-\nu^2)d}} \qquad \text{Equation 2.2}$$

where τ_e = effective shear stress, τ_y = the yield stress, τ_i = lattice friction stress, ν is Poisson's ratio and E is Young's elastic modulus. This model indicates that the fracture of the material should depend primarily on the shear stress acting on the slip band but is also grain size dependent through a $d^{-1/2}$ relationship .

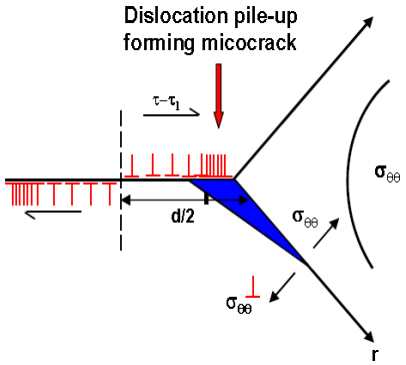

Figure 2.10. Stroh's model for cleavage fracture.

2.5.2 COTTRELL'S THEORY

Cottrell [38] proposed that a dislocation mechanism for the cleavage fracture process should be controlled by the critical crack growth stage under the applied tensile stress. This model showed that the crack's nucleation stress can be small if the microcrack is initiated by the intersection of two low energy slip dislocations to provide a preferable cleavage plane, Figure 2.11.

$$\frac{a}{2}[\bar{1}\bar{1}1] + \frac{a}{2}[111] \rightarrow a[001] \qquad \text{Equation 2.3}$$

This results in a wedge cleavage crack on the (001) plane which is the usual cleavage plane in ferritic materials. Further propagation of the crack is then controlled by the applied tensile stress. As the dislocation reaction in Equation 2.3 is accompanied by a

decrease in dislocation energy, crack nucleation will be easier than if it occurs by the Zener/Stroh mechanism.

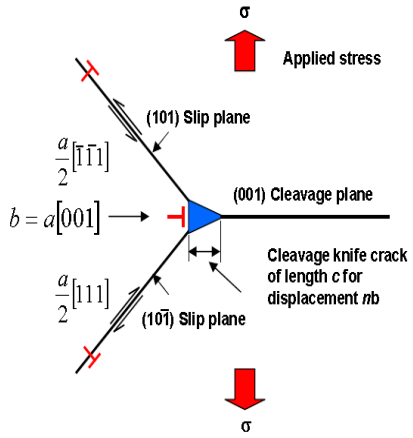

Figure 2.11. Cottrell's model for cleavage fracture.

Cleavage fracture will now be propagation controlled with the cleavage fracture stress, σ_f given by:

$$\sigma_f \geq \frac{2\gamma G_m}{k_y^s} d^{-\frac{1}{2}} \qquad \text{Equation 2.4}$$

where d is the grain size and k_y^s is the Hall – Petch constant for shear. The value of γ calculated was about 20 Jm^{-2}, i.e. about an order of magnitude greater than the surface energy of the lattice. Cottrell attributed this large value to extra work done in producing river lines or transversing grain boundaries [41]. The critical conditions for crack nucleation at the yield stress ($\sigma_f = \sigma_y$) can be expressed by the Cottrell equation [38] as:

$$\sigma_y k_y^s d^{\frac{1}{2}} = k_y^{s\,2} + \sigma_i k_y^s d^{\frac{1}{2}} \geq C_1 G_m \gamma \qquad \text{Equation 2.5}$$

where σ_y is yield stress, σ_i is friction stress, G_m is shear modulus, γ is effective surface energy of an implied crack, C_1 is constant related to the stress state (~4/3 for a notched specimen and 4 for a plain or unnotched specimen). Cottrell's model therefore emphasises the role of tensile stress and explains effects of grain size and yielding parameters on fracture. Hardening, other than by decreasing grain size, is predicted to promote brittle fracture by raising the value of tensile stress at the yield point.

Equation 2.5 expresses the conditions for plastically induced crack nucleation at a given temperature. Any factor that increases σ_i, k_y^s, or d increases the tendency for brittle

fracture. In ferritic steel, a marked increase in σ_i with decreasing temperature is usually experienced. The parameter k_y^s may depend upon alloy content, test temperature or heat treatment. Generally, k_y^s will increase with the stacking fault energy, hence it will be sensitive to alloying. It is obvious from Equation 2.5 that grain size has a direct effect on the transition temperature, and thus, the expression for DBTT at which the fracture stress (σ_f) and yield strength (σ_y) are equal for only one grain size d^* could be derived. Thus

$$DBTT = \frac{1}{\beta}\ln\left[Bk_y d^{*\frac{1}{2}}/(C_1 G_m \gamma - k_y^{s2})\right] \qquad \text{Equation 2.6}$$

For a given material, the relation between transition temperature and grain size may, therefore, be reduced to:

$$DBTT = D + 1/\beta \ln d^{*\frac{1}{2}} \qquad \text{Equation 2.7}$$

where D is a constant. Thus it can be predicted from Equation 2.7 that the temperature at which a DBTT behaviour occurs, decreases with smaller grain size. Plumtree and Gullberg [21] have shown that the DBTT increased linearly with grain size and that the DBTT of lower purity alloys tended to be less affected by grain size changes.

Sometimes the presence of precipitates at grain boundaries camouflages the effect of grain size on the impact toughness of the ferritic stainless steel. The heat treatment that accelerates the precipitation of the carbide and nitride, Laves or sigma phases decreases the resistance to crack initiation significantly during dynamic loading. The V–notched samples embrittled by these precipitates were found to show a toughness behaviour similar to that of the solution treated and sharply notched specimens [42]. Therefore, the precipitates assist greatly in the initiation of brittle cracks at the time of dynamic loading [20]. The DBTT increases with the volume fraction of grain boundary precipitates, thereby facilitating fracture by decreasing the surface energy for fracture (γ). Such grain boundary precipitates can act as starting or initiation points for fracture causing a marked increase in the transition temperature.

Brittle failures are typical transgranular cleavage fractures which occur in the body – centred cubic (BCC) metal at low temperatures and high strain rates. Plumtree and Gullberg [21] proposed the following model which applies only to the initiation of

cleavage cracks. Crack nucleation occurs when the concentrated stresses at the tip of a blocked dislocation band equal the cohesive stress and is given by:

$$(\tau_N - \tau_i)\, nb = 2\gamma_T \qquad \text{Equation 2.8}$$

Where τ_N = shear stress for crack nucleation, τ_i = friction shear stress, n = number of dislocations in the pileup, b = burgers vector, and γ_T = true surface energy.

Equation 2.8 indicates that a crack will form when the work done by the applied shear stress $(\tau_N\, nb)$ in producing a displacement nb equals the combined work done in moving the dislocations against the friction stress $(\tau_i\, nb)$ and the work done in creating the new fracture surface $(2\gamma_T)$. In most metals where some relaxation occurs around the blocked dislocation band, the term γ is used rather than γ_T as grain boundaries, hard particles and of course, grain boundary particles act as barriers to dislocation motion, favouring crack initiation. When the second phases are inhomogeneously distributed the value of γ is reduced [43]. Subsequently the amount of work done in crack nucleation is reduced. Transgranular cleavage cracks form more easily and the toughness is reduced, compared with those alloys where γ remains high due to the second phase distribution.

2.5.3 SMITH'S THEORY

This is an alternative model that provides the starting point for growth – controlled cleavage fracture, to incorporate the effect of brittle second phase particles on grain boundaries, see Figure 2.12. Here, a brittle particle of thickness C_o at the grain boundary dividing adjacent grains, is subjected to the concentrated stress ahead of a dislocation pile – up of length D. A microcrack is initiated when a sufficiently high applied stress causes local plastic strain within the ferrite grains to nucleate a microcrack in the brittle grain boundary particle of thickness C_o. Applying Stroh's analysis, the particle will crack under the influence of the resulting dislocation pile – up if:

$$\tau_e \geq \left\{ \frac{4E\gamma_e}{\pi d\left(1-\nu^2\right)} \right\}^{\frac{1}{2}} \qquad \text{Equation 2.9}$$

where γ_e is the effective surface energy of the particle. Similarly, nucleation controlled cleavage of the ferrite will occur (at the yield point) if:

$$\tau_e \geq \left\{ \frac{4E\gamma_f}{\pi d\left(1-\nu^2\right)} \right\}^{\frac{1}{2}}$$ Equation 2.10

where γ_f is the effective surface energy of ferrite. If, however, τ_e lies between these two limits and γ_f is greater than γ_e, then propagation controlled cleavage fracture is predicted with the particle's microcrack propagating into the ferrite under the combined influence of the dislocation pile – up and the applied stress. By examining the change in energy with crack length, the cleavage fracture stress, σ_f, is given by the following expression leading to an inequality expression predicting growth or propagation of the initiated crack:

$$\sigma_f^2\left(\frac{C_o}{d}\right)+\tau_e^2\left\{1+\frac{4}{\pi}\left(\frac{C_o}{d}\right)^{1/2}\frac{\tau_i}{\tau_e}\right\}^2 \geq \frac{4E\gamma_f}{\pi d\left(1-\nu^2\right)}$$ Equation 2.11

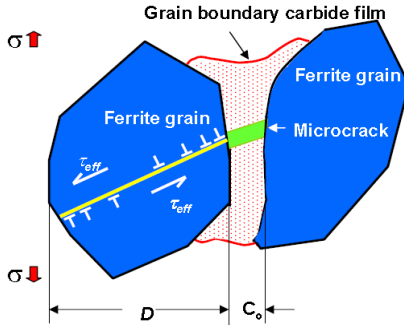

Figure 2.12. Smith's model for cleavage fracture.

In the absence of a contribution by the dislocations (the second term in Equation 2.11) the inequality expression is reduced to:

$$\sigma_f > \left[\frac{4E\gamma_f}{\pi(1-\nu^2)C_o} \right]^{\frac{1}{2}}$$ Equation 2.12

This model, therefore, emphases the importance of the precipitate's thickness C_0 and indicates clearly that the coarser particles give rise to lower fracture stresses. If, however, the effective shear stress τ_e is written as $k_y^s d^{-1/2}$, the equation predicts that σ_f is independent of grain size, other factors being equal. Indirectly, however, the grain size will determine the value of C_0 for a given volume fraction of the grain boundary phase and, therefore, does exert an indirect influence on the fracture strength. In

practice, therefore, a fine grain size with a large grain boundary area per unit volume, is associated with thin precipitates, and values of σ_f are usually expected to be high with smaller grain sizes.

2.5.4 CLEAVAGE FRACTURE RESISTANCE

Analyses of the factors controlling the cleavage fracture stress have been made previously by different authors [44]. Although the fracture process in the steel does not, in general, correspond to the condition for which these expressions were derived (that is, fracture is frequently initiated at the tip of a stopped microcrack or by the joining of several microcracks by tearing), directly analogous expressions should exist for these conditions. From Equation 2.13, it should be noted that the fracture stress depends on the grain size, as well as yield strength, and that refining the grain size increases both of them.

$$\sigma_f = \left(8G_m\gamma_m / k_y\right)d^{-\frac{1}{2}} \qquad \text{(clean material)} \qquad \text{Equation 2.13}$$

$$\sigma_f = \left[\frac{2E\gamma_b}{\pi\alpha\left(1-\nu^2\right)}\right]^{\frac{1}{2}} d^{-\frac{1}{2}} \qquad \text{(less pure material)} \qquad \text{Equation 2.14}$$

where G_m and E are the shear and Young's moduli, respectively, γ_m and γ_b are the appropriate surface energy terms, ν is Poisson's ratio and α is a constant.

The most probable important environmental factor that affects the failure of the materials is the service temperature. Although many different criteria exist for the conditions of a DBTT, they all effectively point to the temperature at which $\sigma_f = \sigma_y$. It has been observed that grain refinement increases both of these stresses.

In the case of solid solution and precipitation strengthening, the ductile to brittle transition temperature is usually raised. This results from these strengthening mechanisms that do not increase the fracture stress, as grain refinement does.

2.6 THERMOMECHANICAL PROCESSING

In the previous section it was mentioned that the toughness of ferritic stainless steel depends on the grain size, and this grain size can be refined by thermomechanical processing. However, a thermomechanical process also affects the recrystallisation parameters and precipitation of carbides, nitrides, sigma and Laves phases [18,45]. The

thermomechanical processes that affect the changes in microstructure of the ferritic stainless steel will be considered in this section.

2.6.1 COLD-ROLLING

Cold rolling was found to raise the DBTT, but the effect is not consistent nor is it very great [18]. Differences in cold rolling temperature and the extent of preferred grain orientation make the effects more difficult to quantify. Sawatani et al [8] have observed the effects of a reduction by cold rolling on the elongation and the amount of Laves phase precipitates present in a Ti and Nb stabilised low C, N-19%Cr-2%Mo alloy. Their results show that at a 20% cold reduction a very large amount of Laves phase is precipitated that increases the strength and decreases the elongation of the steel. Cold rolling is considered to give a high enough dislocation density to nucleate these Laves particles at dislocations and not only at grain boundaries. The optimum properties of cold rolled and annealed steel of this composition are obtained by cold reduction of more than 80%, followed by annealing at 920 °C, which will dissolve the Laves phase, followed by rapid cooling.

2.6.2 HOT-ROLLING

Ferritic stainless steel can be hot-rolled without difficulty. However, grain refinement during the hot-rolling process does not occur readily and the grain structure can be quite coarse, particularly after relatively high finishing temperatures. Hot-rolling may also accelerate the precipitation of the Laves phase. It is thus imperative not to hot work in the temperature range of the stable Laves phase precipitation in these steels. After hot rolling, the steel is usually rapidly cooled from the temperature range of 900 to 950 °C to prevent the formation of the Laves phase during cooling. Care must also be exercised when working with high interstitial content alloys, since hot-rolling at high temperatures and quenching can lead to high temperature embrittlement [46].

2.6.3 COOLING RATE

The cooling rate affects the intensity of the precipitate's formation by altering its nucleation rate. Fast cooling rates can prevent precipitation; intermediate cooling rates cause maximum age-hardening, while slow cooling rates give over-ageing which produces low strength. If the precipitation has been suppressed during cooling, it can be induced during the ageing process [47,48].

2.6.4 HEAT TREATMENT

Heat treatment is a major factor in controlling the properties of stainless steels. The ferritic steels are annealed at temperatures from 750 to 900 °C, and the upper limit should not be exceeded substantially since grain growth will induce a decrease in toughness [49]. However, by keeping (C + N) levels very low, concern about grain – size related DBTT increases can be prevented [18]. Annealing must be followed by rapid cooling to avoid prolonged exposure to the temperatures at which Laves phase will form or "475 °C" brittleness will develop.

With total (C + N) content below approximately 500 ppm, quenching generally produces optimum toughness by preventing sigma or Laves phase precipitation as well as carbide and nitride precipitation. With higher (C + N) levels, nothing is gained by quenching and if a high temperature anneal is used, rapid quenching can cause embrittlement by severe carbide and nitride precipitation. This rapid cooling embrittlement can be reduced substantially by the addition of carbide and nitride stabilisers, such as Nb and Ti.

2.7 APPLICATIONS OF STAINLESS STEELS IN AUTOMOBILE EXHAUST SYSTEM

Recently, environmental pressures have required the reduction of dangerous exhaust gas emissions from motor cars, and there has been an effort by automobile manufacturers to raise the temperature of exhaust gases from automobile engines to about 900°C in order to give a cleaner exhaust gas [50, 51]. To improve the efficiency of the automobile engines and to reduce their weight, more conventional stainless steel sheets and tubes in the application of exhaust systems are now replacing the traditional cast iron, particularly in near-engine applications. The exhaust system is divided into two main parts, the hot and the cold ends. The components of the hot end consist of the exhaust manifold, front pipe, flexible pipe and catalytic converter and the components of the cold end consist of a centre pipe main muffler and tail end pipe, see Figure 2.13. Typical operating temperatures and the current materials used for these different components are shown in Table 2.1.

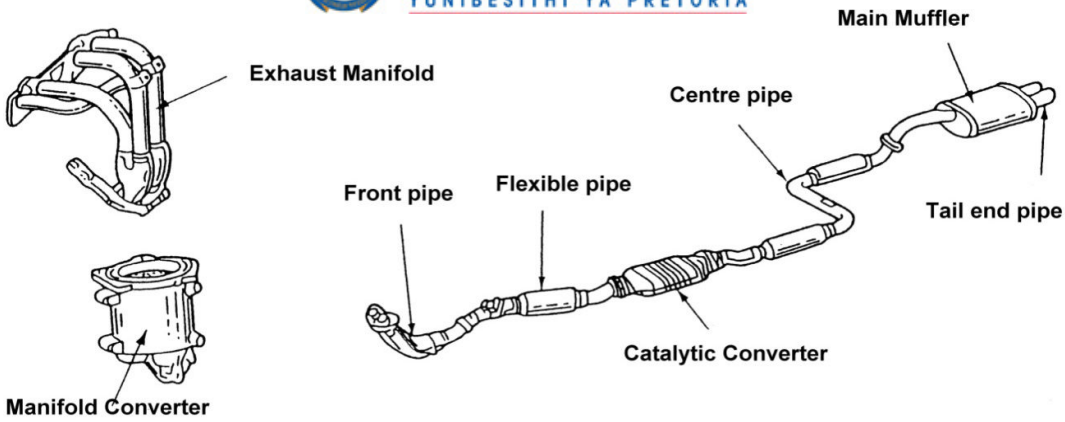

Figure 2.13. Automobile exhaust system components.

Table 2.1. Component of automobile exhaust system and their typical operating temperatures [52,53,54].

Component		Service temp (°C)	Required properties	Current materials
Exhaust manifold		950 – 750	• High temperature strength • Thermal fatigue life • Oxidation resistance • Workability	409, 441, 304, 321, 309
Front pipe		800 – 600		304, 321,309, 409
Flexible pipe				304, 321, 309 and 316Ti
Catalytic converter	Shell		• High temperature strength • High temperature salt damage resistance • Workability	441, 409, 321, 309
	Catalyst carrier*	1000 – 1200	• Oxidation resistance • Thermal shock resistance	
Centre pipe		600 – 400	• Salt damage resistance	304, 409, 441
Main muffler		400 - 100	• Corrosion resistance at inner surface (condensate) • Corrosion resistance at outer surface (salt damage)	409, 434, 436, 430Ti, 321, 304
Tail end pipe				304, 316

Thus, the materials for automobile exhaust systems require excellent thermal fatigue resistance and higher temperature strength. Ferritic stainless steels are the commonly used materials in exhaust systems as a compromise between inexpensive carbon steels and the higher cost of higher alloyed ferritic or austenitic steels. Ferritic stainless steels have better corrosion resistance and thus a longer life than low carbon steels and have lower cost than the more highly alloyed stainless steels. However, ferritic stainless steels have relatively low strength at elevated temperatures compared to austenitic steels. Therefore, efforts have been made to create new ferritic stainless steels with

* The catalyst carrier are usually made out of ceramic, there has been a recent development in metal carrier made out of ferritic stainless steel foils because they have good thermal shock properties and a small heat capacity [53].

excellent thermal fatigue resistance and high strengths at elevated temperatures. This has been achieved by the use of stabilising elements such as the addition of niobium and titanium, as will be discussed in the next section.

2.8 Heat Resistant Ferritic Stainless Steels

Niobium-containing ferritic stainless steels are being used in automotive exhaust systems because of their excellent heat resistant properties, especially their thermal fatigue resistance which is very important for materials of exhaust systems because of the frequent heating and cooling cycles. When in solid solution, the Nb addition increases the initial high temperature strength compared with other alloying elements, see Figure 2.14 below [4]. However, Nb forms several types of precipitates during service, which can cause degradation in high temperature strength and thermal fatigue resistance [3].

In the work by Fujita et al. [5], the effect of Nb additions in 0.01C – 0.01N – 13Cr steel on the 0.2% proof strength at 900 °C is observed to be effective above 0.2 %wt Nb. On the other hand, Mo additions increase the high temperature strength approximately in proportion to the alloy addition content.

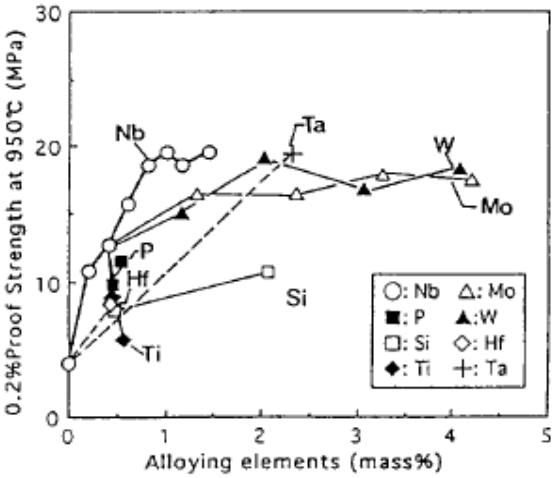

Figure 2.14. Effect of alloying element additions on the 0.2% proof strength at 900 °C of a 13%Cr ferritic steel [4].

2.9 Stabilisation

To combat the problem of sensitisation, the carbon in stainless steels is reduced through a combination of steelmaking practices and through the addition of elements with strong

affinity for carbon and nitrogen. Firstly, these steels are processed by an "argon-oxygen decarburisation (AOD)" or "vacuum-oxygen decarburisation (VOD)" process to reduce the carbon content to very low levels (<0.02%C). The carbon and nitrogen in solution are further reduced through the addition of stabilising elements such as titanium (Ti) and niobium (Nb), tantalum (Ta), vanadium (V) and molybdenum (Mo). These elements form carbides, nitrides or carbo-nitrides and precipitate at higher temperatures and shorter times than chromium carbides, thus removing most of the carbon and nitrogen from solution before the chromium carbides form. Because of the high cost of Ta, it is normally not used in the stabilisation of stainless steels. Either Nb or Ti individually and/or Ti plus Nb additions have been used in stainless steels for automobile exhaust systems, and the two stabilisation methods will be compared in the next section.

2.9.1 Stabilisation with Titanium

This is the most widely used stabilising addition to stainless steels. The highly reactive element forms highly stable titanium nitride (TiN) precipitates in the presence of N and titanium carbide (TiC) in the presence of C. Whilst in the presence of both nitrogen and carbon, titanium carbonitride (Ti(C,N)) is formed owing to the mutual solubility of TiN and TiC [55]. The ratio of TiC/TiN in the Ti(C,N) is dependent upon the ratio of N/C in the alloy. In Ti stabilisation practice it is generally accepted that the level of Ti required to fully-stabilise a stainless steel is directly dependent on the C and N content, and can be calculated empirically from [55]:

$$Ti=0.2 + 4(C+N)$$

The disadvantage of Ti stabilisation is that Ti-stabilised stainless steel suffers from surface defects that require surface grinding and these result in an increase in the overall production cost. This can be overcome by combining Ti additions with other stabilising elements such as aluminium (Al), niobium (Nb) or vanadium (V).

2.9.2 Stabilisation with Niobium

Many researchers have investigated the effects of niobium stabilisation on ferritic stainless steels for their use in automotive exhaust systems [3,4,5,6] and have found that niobium additions can improve the high temperature strength of ferritic stainless steels by solid solution strengthening, which allows its operation at such high temperatures. Generally, solute Nb readily precipitates out as a carbo-nitride when the steel is used at high temperatures of about 900°C for long times [3,4]. In addition to its

stabilisation effects, small amounts of Nb in the stainless steel have been known to affect both mechanical and microstructural properties [6]. It is, therefore, important to know how much of the niobium precipitates out as carbides or as carbo-nitrides and which fraction remains in solution. Niobium stabilised ferritic stainless steels form the carbide precipitates NbC, M_6C (Fe_3Nb_3C) and the Laves phase type Fe_2M (Fe_2Nb). The main benefit of the Nb is its ability to suppress recovery, recrystallisation and grain growth in ferritic steels [4].

2.9.3 Solid Solution Hardening and Solute Drag by Niobium

Niobium addition is the most frequently used microalloying element because it has a significant effect on the microstructure and the mechanical properties of ferritic stainless steels. Depending on the state of Nb (in solid solution or in precipitates) as determined by the heat treatment, Nb has a significant effect on the recrystallisation and the grain growth. The effect of Nb on the recrystallisation and the grain growth of the austenite has been widely studied [56,57,58]. Nb addition, even in small amounts, can lead to a significant decrease in grain boundary mobility, as well as an increase in the recrystallisation temperature. Both the decrease in the grain boundary mobility and increase in the recrystallisation temperature might be caused by a solute drag effect of Nb in solid solution and the pinning effect of fine precipitates such as NbC and Fe_2Nb. Suehiro [57] has shown that Nb retards the migration of grain boundaries during recrystallisation due to the solute drag effect.

The quantitative theory of the solute drag effect on a moving grain boundary during recrystallisation was originally formulated by Lücke and Detert [59]. It was later modified by Cahn [60] and then by Lücke and Stüwe [61]. Since then, this theory has been further refined by several authors [57,58,62]. The equation proposed by Cahn on the rate of grain boundary movement as it is affected by solute drag is [63,64]:

$$\frac{p_d}{v_b} = \frac{1}{M_T} = \frac{1}{M_0} + \frac{\alpha X_s}{\left(1+\beta^2 v_b^2\right)} \qquad \text{Equation 2.15}$$

where p_d is the driving force for the grain boundary mobility and v_b is the mobility rate, M_T is the overall mobility due to intrinsic plus solute drag, M_0 is the intrinsic grain boundary mobility in pure material, X_s the atom fraction of solute in the bulk metal, α is a term related to the binding energy of solute to the grain boundary and β is a term related to the diffusivity of the solute in the vicinity of the grain boundary.

In the work by Le Gall and Jonas [63], the authors have determined the effect of solute concentration and temperature on the grain boundary mobility against driving force using the Cahn model. Their results show that; at high concentrations and low temperatures, the mobility of the grain boundary is low and if the driving force or the temperature is increased, the increase in mobility is very significant and tends towards that of pure metals. The overall results are described by curves with approximately two slopes; M_0 representing the intrinsic mobility in the pure metal and M_B which refers to the mobility in the presence of solute drag elements.

Hillert and Sundman [65,66] developed a theory that is most general because the validity of the theory is not limited to the dilute solution case and it can be applied to both grain boundary and phase interface migrations. Suehiro et al.[58] developed the simplified model to calculate the solute drag effect on a moving phase interface, but it can also be applied to both grain boundaries and phase interfaces. They applied this model to the phase transformation in an Fe-Nb system [57]. In this model, recrystallisation is described as a phase transformation for which the driving force results from the energy stored as dislocations. It should also be mentioned that the stored energy in a plastically deformed material may give rise to the driving force for grain boundary migration in recrystallisation through the Strain Induced Boundary Migration (SIBM) mechanism.

It was shown that the Cahn equation (that is, Equation 2.15) can be simplified when the driving forces are low [63]. The overall mobility due to intrinsic plus solute drag is then given by:

$$\frac{1}{M_T} = \frac{1}{M_0} + \frac{1}{M_B} \qquad \text{Equation 2.16}$$

where M_0 is the intrinsic mobility in a pure metal and M_B is the grain boundary mobility under solute drag conditions. The solute drag equation is then reduced to:

$$v_b = M_T p_d \qquad \text{Equation 2.17}$$

This equation is only valid for low driving force phenomena such as grain growth, whereas with higher driving forces as with the recrystallisation, Le Gall and Jonas [63] proposed a “law of mixtures”:

$$M_T = M_0(1-f_{GB}) + M_B f_{GB} \qquad \text{Equation 2.18}$$

where M_0 and M_B are defined as above, f_{GB} is a function of potential grain boundary sites filled by solute and is temperature dependent.

2.9.4 Effects of Temperature on Solute Drag

The effect of temperature on solute drag during recrystallisation has been investigated in an Fe-Nb alloy [57]. These results show that Nb decreases the velocity of the recrystallising grain boundary at the composition covering the critical composition and this depends on the temperature and total driving force. This retardation was found to be caused by the solute drag effect of Nb. In work by Suehiro et al. [58], the author studied the effect of Nb on the austenite to ferrite transformation in ultra low carbon steel. Their results indicate that there is a critical temperature where the rate of transformation changes drastically. The transformation that occurs above and below the critical temperature are both partitionless massive transformations. The critical temperature was found to be composition dependent, and for the 0.25% Nb alloy it was found to be 760 °C and for 0.75%Nb alloy it was 720 °C

From Equation 2.15, however, it can be predicted that by increasing the temperature to the point where the mobility of solute atoms becomes high, solute drag becomes less effective and the overall mobility parameter approaches the intrinsic mobility factor, that is $M_T \approx M_0$. . Le Gall and Jonas [63] have observed solute drag by sulphur atoms in pure nickel, while observing that the transition from solute drag to purely intrinsic mobility of the grain boundary is not a gradual one but that it occurs at a critical temperature that provides a “break” in the mobility versus inverse temperature relation.

2.9.5 Dual Stabilisation with Titanium and Niobium

Research conducted over the last few decades has revealed the benefits of stabilising carbon and nitrogen by using both titanium and niobium. These observations led to the development of the modern generation of ferritic stainless steels, i.e., dual-stabilised ferritic stainless steel. The dual stabilisation imparts beneficial corrosion resistance, oxidation resistance, high temperature strength and formability to the steel [2,31]. At present, it appears to be well accepted that to achieve full stabilisation of ferritic stainless steels a ratio of Nb:Ti = 2:1 is preferred [31]. The optimum limits of dual stabilisation have been established experimentally, and are given by:

Ti + Nb = 0.2 + (C + N) at min

Ti + Nb = 0.8 at max

To reduce grain growth during high temperature annealing extra niobium is added, leading to intermetallic precipitation. The addition of titanium and niobium is made in such a way that an extra content of niobium (ΔNb) is kept in solid solution after the carbo-nitride precipitation [67]:

$\Delta Nb = [Nb] - 7([C] + [N])$ in case of Nb stabilisation

$\Delta Nb = [Nb] - 7/2\ [C]$ in case of (Ti + Nb) stabilisation

At temperatures between 600 and 950 °C, isothermal treatment has shown that the residual niobium precipitates out to form intermetallic Fe_2Nb. Schmitt [67] has observed that depending on the temperature, a part of the precipitation occurs on the grain boundaries combined with a fine intergranular precipitation, and this strongly slows down the grain boundary mobility. The nature of the precipitates, the size and location depends also on the alloy composition. The value of the excess ΔNb content is significant, as well as the silicon and molybdenum content. Both the Si and Mo have an effect to enhance the precipitation of the Laves phase [29].

2.10 AISI Type 441 Stainless Steels

Type 441 alloy is a low carbon, Ti and Nb stabilised, heat resisting ferritic stainless steel providing good oxidation and corrosion resistance for applications such as automotive exhaust system components. The high chromium content makes type 441 steel far more corrosion resistant than its counterpart type 409 [52]. The 441 steel is dual stabilised with niobium and titanium to provide good weld ductility and resistance to intergranular corrosion in the weld's heat affected zone. Type 441 is manufactured according to the requirements of EN 10088-2 and certified as 1.4509, see Table 2.2 for its chemical composition.

The structure of type 441 is a completely ferritic alloy, i.e. the matrix has a body centred cubic crystal structure up to its liquidus temperature. Angular carbo-nitrides of titanium and niobium that have precipitated from the melt are randomly dispersed throughout the structure. The presence of the titanium nitrides and carbides in the steel tends to lower the melting point of the steel, as shown by Gordon [55], see Figure 2.15. Excess niobium is taken into solid solution during high temperature annealing and precipitates as very fine particles of Laves phase (Fe_2Nb) upon either slow cooling or upon holding

at intermediate temperatures of 600 – 950 °C [68]. Strengthening by this dispersion is responsible for improved elevated temperature strength [69].

Table 2.2. Chemical composition of type 441 stainless steel in accordance with EN 10088-2 [70].

	C	N	Mn	Si	Cr	Ni	Ti	Nb	S	P	Remarks
Min					17.50		0.10				%Nb≥ 3xC + 0.3
Max	0.03	0.045	1.00	1.00	18.50	0.50	0.60	1.00	0.015	0.04	

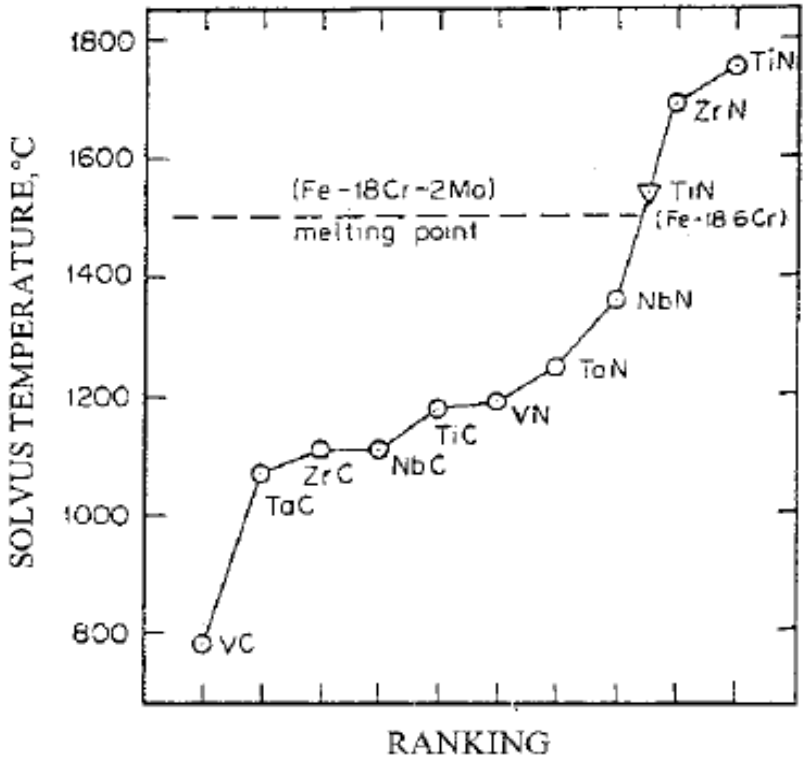

Figure 2.15. The solvus temperatures of the precipitates found in stabilised ferritic stainless steels [55].

2.11 CALPHAD METHODS

The CALPHAD (CALculations of PHAse Diagram) method primarily uses numerical techniques based on thermodynamic principles for addressing complex problems like stable and metastable phase equilibria in the multicomponent systems for equilibrium conditions. The essence of the Calphad approach is to obtain the parameters of thermodynamic models for the Gibbs energies of the constituent phases in terms of known thermodynamic and phase equilibrium data in the lower order systems, binaries and ternaries. The Gibbs energies of multicomponent alloy phases can be obtained from those of lower order systems via an extrapolation method [71]. These Gibbs energy values enable engineers and scientists to calculate reliable multicomponent phase diagrams in many instances. Experimental work is then only required for

confirmatory purposes and not for the determination of the entire phase diagram. The Calphad approach in calculating phase diagrams of multicomponent alloy systems is shown schematically in Figure 2.16 [71].

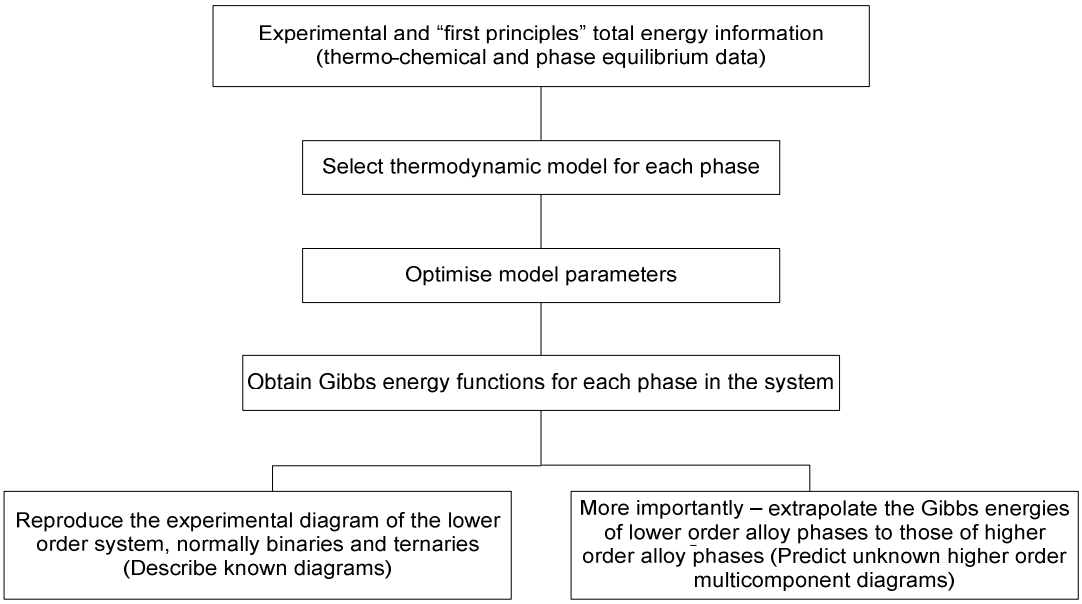

Figure 2.16. Schematic flow diagram showing the Calphad approach used to obtain a thermodynamic description of a multicomponent system.

Thermodynamic descriptions of the constituent lower order systems, normally binaries and ternaries, are obtained through experimental and "first principles" of total free energy information and phase equilibrium data [72]. However, once descriptions for the lower order systems are known, it is possible in many cases to obtain thermodynamic descriptions of the higher order systems by using an extrapolation method so that more complete phase diagrams of the system can be calculated.

The Gibbs energy of a phase is described by a model that contains a relatively small number of experimentally optimised variable coefficients. Examples of experimental information used include melting and other transformation temperatures, solubilities, as well as thermodynamic properties such as heat capacities, enthalpies of formation and chemical potentials.

For pure elements and stoichiometric compounds, the following model is commonly used:

$$G_m - H_m^{SER} = a + b \cdot T + c \cdot T \cdot ln(T) + \sum d_i \cdot T^i \qquad \text{Equation 2.19}$$

where, $G_m - H_m^{SER}$ is the Gibbs energy relative to a standard element reference state (SER), H_m^{SER} is the enthalpy of the element in its stable state at the temperature of

298.15 Kelvin and a pressure of 10^5 Pascal (1 bar), and a, b, c, and d_i are model parameters.

For multi-component solution phases, the following expression for the Gibbs energy is used:

$$G = G^{\circ} + {}^{id}G_{mix} + {}^{xs}G_{mix} \qquad \text{Equation 2.20}$$

where G° is the Gibbs free energy due to the mechanical mixing of the constituents of the phase, ${}^{id}G_{mix}$ is the ideal mixing contribution, and ${}^{xs}G_{mix}$ is the excess Gibbs energy of mix (the non-ideal mixing contribution).

If a phase in a multi-component solution is described with a single sub-lattice model, then the G°, ${}^{xs}G_{mix}$ and ${}^{xs}G_{mix}$ contributions to the Gibbs energy can be expressed as follows:

$$G^{\circ} = \sum_i c_i \cdot G_j^{\circ} \qquad \text{Equation 2.21}$$

$${}^{id}G_{mix} = R \cdot T \cdot \sum_i c_i \cdot ln(c_i) \qquad \text{Equation 2.22}$$

$${}^{xs}G_{mix} = \sum_i \sum_{j>i} c_i \cdot c_j \cdot \sum_k L_{i,j}^k \cdot (c_i - c_j)^k \qquad \text{Equation 2.23}$$

where c_i and c_j are the mole fraction of species i and j respectively, and $L_{i,j}^k$ is a binary interaction parameter between species i and j. The binary interaction parameter $L_{i,j}^k$ is dependent on the value of k. When the value of k equals zero or one, the equation for ${}^{xs}G_{mix}$ becomes regular or sub-regular, respectively.

2.11.1 THERMODYNAMIC SOFTWARES

During the last few decades, the rapid development of thermodynamic and kinetic software packages, such as Thermo-Calc®, DICTRA [73,74], ChemSage, FactSage and MTDATA have made it possible to calculate complex phase equilibria in multicomponent systems. It is evident that gradually the accuracy of these calculations will become more and more dependent on the databases behind the packages. So far, a great number of binary, ternary and even quaternary systems have been assessed to obtain a sufficiently sound database for multicomponent steels [75,76,77]. However, there are still some subsystems not assessed earlier or assessed but not shown in the open literature.

2.12 INTERMETALLIC LAVES PHASE

2.12.1 CRYSTALLOGRAPHIC STRUCTURE

Many intermetallic phases belong to the group of the Laves phase with AB_2 compositions of topologically close packed (TCP) structures. Furthermore, these Laves phases are capable of dissolving considerable amounts of ternary alloying elements [78,79,80]. Laves phases are generally stabilised by the size factor principles, that is, the atomic size ratio r_A/r_B, which is ideally 1.225 with a range of 1.05 - 1.68 that is usually observed [81,82]. Three types of Laves phase (see Figure 2.17 [85]) and the Pearson symbols and their crystallographic structures are given below [83,84,85,86]:

Table 2.3. Crystallographic structure and the space groups of the three types of the Laves phase.

Typical composition	Structure	Pearson symbol	Space group	Space group number
C14, $MgZn_2$	hexagonal	*h*P12	$P6_3/mmc$	194
C15, $MgCu_2$	fcc	*c*F24	$Fd\bar{3}m$	227
C36, $MgNi_2$	hexagonal	*hP24*	$P6_3/mmc$	194

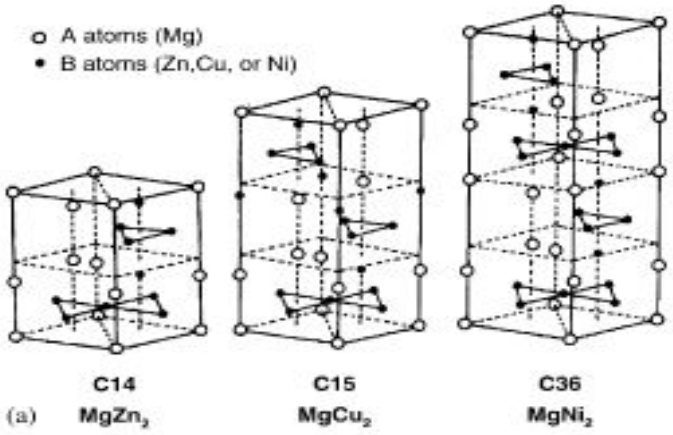

Figure 2.17. The three polytypes of the Laves phase structure in a hexagonal setting.

The Fe_2Nb Laves phase (Mg_2Zn type, C14) is a hexagonal close packed phase with the space group $P6_3/mmc$, and the lattice parameters of a=0.473 nm and c=0.772 nm with c/a = 1.633. The main factor determining its formation is the relative atomic size of the constituent atoms, with the ranges of composition quite small. This Laves phase probably does not form at its exact equilibrium composition [8,87]. In Nb and/or Ti stabilised stainless steel grades, Fe_2Nb or Fe_2Ti (more seldom) can form.

2.12.2 Occurrence

The precipitation rate of the Laves phase in a Ti and Nb stabilised steel was observed to reach a maximum at 700°C and its dissolution occurs at temperatures over 900°C [88]. The same observation has been made by the use of thermodynamic software such as Thermo-Calc® [3] and its growth and coarsening rates have been simulated by Bjärbo [9] using DICTRA software. The Laves phase precipitates firstly on sub- and grain boundaries as a fine precipitate and as the steel is slowly cooled from a high temperature of about 900°C, the amount of Laves phase increases but now inside the grains and the particles then coarsen. In the work by Murata et al, [89] they have shown that the Laves phase's solvus temperature depends on the content of the alloying elements, that is, the solvus temperature increases with increasing alloying content.

The intermetallic Laves phase is known to affect the mechanical properties and corrosion resistance of ferritic stainless steel. It has been found that a fine precipitate of Laves phase at grain boundaries improves the high temperature strength when still fine [6]. However, rapid coarsening of the Laves phase at high temperatures reduced the high temperature strength [10] although the exact mechanism is still not clear and still requires clarification. In research done by Fujita et al.[5] to determine the solubility products in a niobium stabilised ferritic steel it was found that a Mo addition enhances the precipitation of the Laves phase even if the addition is as small as 0.5mass%Mo. Sawatani et al [11], studied the effect of Laves phase on the properties of dual stabilised low carbon stainless steels as related to the manufacturing process of Ti- and Nb-stabilised low (C, N)-19%Cr-2%Mo stainless steel sheets, and have found that the Laves phase has a significant influence on the mechanical properties of the steel. It was found that Laves phase on the grain boundaries shifts the brittle to ductile transition temperature to a higher temperature, and large amounts of Laves phase degrade the room temperature ductility of cold rolled and annealed sheet and greatly enhances its strength. It was also observed that after a 20% cold rolled reduction (of the sheet that was cold rolled and annealed after 0 to 92% reductions) that there was a peculiarly rapid precipitation of Laves phase, which caused a severe degradation of the mechanical properties [8]. The reason for the rapid increase in Laves phase precipitation was not clear, but it was assumed that there is possibility that an autocatalytic reaction occurs to substantially increase the precipitation rate of Laves phase. The rate of autocatalytic reaction under which the nucleation and growth of

particles occur at dislocations will greatly depend on the formation rate of new dislocations from the cold work which then act as new precipitation sites.

2.12.3 Orientation Relationship

Cocks and Borland [90] have investigated the orientation relationship and morphology of Fe_2Nb precipitates within the ferrite matrix in 0.6 at%Nb and 1.9 at%Nb alloys respectively, using electron diffraction techniques. They had found that there exists a single orientation relationship:

$$\{11\bar{2}0\}_{Fe_2Nb} // \{111\}_{\alpha} : \langle 0001 \rangle_{Fe_2Nb} // \langle 112 \rangle_{\alpha} \qquad \text{Equation 2.24}$$

and the morphology of these particles are disc-shaped lying on the $\{111\}_{\alpha}$ plane. Lath-shaped particles were found to have developed in overaged alloys and most of these particles tend to be elongated in the $\langle 112 \rangle$ matrix direction. The orientation relationship between the rod-like Laves phase particles and the matrix was found to be [11,91]:

$$\{11\bar{2}0\}_{Fe_2Nb} // \{111\}_{\alpha} : \langle 0001 \rangle_{Fe_2Nb} // \langle 110 \rangle_{\alpha} \qquad \text{Equation 2.25}$$

The analysis suggests that the habit plane, if any, must be $\{110\}_{\alpha}$ and the preferred growth direction must be $\langle 110 \rangle_{\alpha}$ [92]. The two orientation relationships are completely different from one another and the habit planes are also different. In work by Miyahara et al. [93] on Fe-10%Cr ferritic alloys, they have observed very small disk–like Laves phase (Fe_2Mo) precipitates that had formed on the $\{100\}_{\alpha}$ plane and which have a coherent strain field in the matrix. Therefore, it may be reasonable to consider that there can be several orientation relationships rather than only one orientation relationship. None of the above authors tried to relate the orientation relationship of the Laves phase to its precipitation morphologies.

In the work done by Murata et al. [94], the authors determined the surface interfacial energy γ_{SF} of the coherent and incoherent Laves phases in the Fe-Cr-W- C quaternary system. They observed that the coherent fine Laves phase has a lower interfacial energy than the incoherent granular Laves phase, and their estimated values were 0.1 J/m^2 and 0.468 J/m^2, respectively. Also, their results show that there is a morphological change of the Laves phase from the fine coherent precipitates to the granular ones. This morphological change occurs in a regular ageing sequence in the steel if it contains more than 4 wt.% W.